Correlation of intrinsic point defects and the Raman modes of cuprous oxide

T. Sander,* C. T. Reindl, M. Giar, B. Eifert, M. Heinemann, C. Heiliger, and P. J. Klar
I. Physikalisches Institut, Justus-Liebig-Universität Gießen, Heinrich-Buff-Ring 16, 35392 Gießen, Germany
(Received 14 March 2014; revised manuscript received 19 May 2014; published 9 July 2014)

The Raman spectrum of crystalline Cu_2O taken off resonance is reproducible and independent of the growth method and conditions employed. But, in contrast to most other crystalline materials, the Raman spectrum of Cu_2O is dominated by infrared active and silent lattice modes rather than by the only Raman allowed phonon mode. We show that this unusual behavior is most likely caused by the presence of copper vacancies in the so-called split configuration, a point defect particular to Cu_2O. The reduction of symmetry due to the presence of point defects may lift the Raman selection rules and may introduce Raman activity for phonon modes that are Raman forbidden in the case of perfect crystal symmetry. Based on this group theoretical consideration, we predict the angle dependence of the Raman intensities of all Cu_2O one-phonon modes at $k = 0$ for rotation about the (100) direction caused by the presence of various intrinsic point defects. Of all intrinsic defects in question, only the presence of the copper vacancy in the split configuration introduces Raman activity for all Cu_2O extended phonon modes observed in experiment and is consistent with the angle-dependent measurements. Our study underlines the special role of the split vacancy in Cu_2O.

DOI: 10.1103/PhysRevB.90.045203 PACS number(s): 78.30.−j, 78.66.Li, 63.20.kp

I. INTRODUCTION

There are no perfect crystals in reality, as entropy always leads to the formation of defects [1]. Even in chemically pure materials, a large variety of intrinsic defects will occur, e.g., point defects such as vacancies, interstitials, or substitutional or antisite defects. Raman spectroscopy is widely employed for studying the vibrational properties of solids. In crystalline samples, it yields information about chemical composition, crystal class, and crystalline orientation, among other properties [2]. The extraction of this information from the Raman spectra is usually based on the assumption of an ideal crystalline structure. For a perfect crystal structure, the detectability of lattice modes in a Raman experiment arises from the laws of conservation of energy and momentum as well as symmetry selection rules. Despite the considerable amount of defects present in crystalline samples, this approach is very successful in most crystalline materials, and their Raman spectra of the extended lattice modes serve as characteristic fingerprints.

What is the impact of defects on the Raman spectra? (i) The occurrence of defects in a crystalline material may cause local vibrational modes, which may lead to additional, usually rather small features in the Raman spectrum [3,4]. Furthermore, the lowering of the symmetry due to the formation of defects may have some consequences according to group theory: (ii) The perfect translational symmetry of the crystal lattice is broken, consequently the wave vector is no longer a good quantum number [5]. The extreme is a glassy or amorphous material, where the loss of long-range order leads to a Raman spectrum that reflects the phonon density of states and wave vector selection rules do not apply anymore. (iii) The Raman selection rules derived for the perfect crystal do not hold strictly any longer, e.g., the point defects reduce the local symmetry such that degenerate modes may split and the assignment of Raman allowed and Raman forbidden lattice vibrations may be lifted. Such changes of degeneracy and Raman activity of lattice modes induced by the incorporation of defects are rarely observed. The reason is that the perturbation due to the defects is usually too small to significantly alter the Raman selection rules.

The cuprous oxide semiconductor Cu_2O is an exception from this rule. The dominant one-phonon signals observed in the Raman spectra of Cu_2O are actually due to modes that are infrared active or silent in perfect crystal symmetry, rather than due to the single Raman active mode of the ideal crystal. This finding is independent of the growth method and synthesis conditions. In this article, we present a group theoretical analysis of the impact of various intrinsic point defects on the local symmetry and thus on the Raman spectrum of Cu_2O. The analysis allows us to identify the one-phonon modes that become Raman active in the presence of a particular defect, and to derive the corresponding altered Raman selection rules. The measured angle dependence of the intensities of the one-phonon Raman signals is compared with theoretical predictions based on these altered Raman selection rules for different point defects. Full agreement is obtained for the copper vacancy in the split configuration only. Furthermore, we employ density functional theory (DFT) calculations for supercells containing a single defect to estimate the magnitude of its perturbation on the Cu_2O lattice.

II. EXPERIMENTAL AND METHOD DETAILS

Raman spectra were recorded in backscattering geometry at room temperature (300 K) and 80 K with a Renishaw inVia Raman microscope. A linearly polarized laser with a wavelength of either 532 or 633 nm was used for excitation and focused onto the sample surface with a 50× objective. The same objective was used to collect the scattered light, which was then dispersed by a spectrometer with a focal length of 250 mm and detected by a charge-coupled device (CCD). The system's spectral resolution is limited to about 1.5 cm^{-1}. To measure the angle-dependent spectra, a microscope stage rotating about the axis defined by the

*Thomas.Sander@physik.uni-giessen.de

direction of the incoming excitation laser was used. Polarizers and waveplates enable measurements in various scattering geometries.

To obtain the phonon dispersion relation and the density of states (DOS), we performed ground-state calculations for supercells within the framework of DFT. We used the Perdew-Burke-Ernzerhof (PBE) parametrization of the generalized gradient approximation (GGA) variant of the exchange correlation potential in combination with the projector augmented-wave method as implemented in the VASP code [6–9]. Harmonic interatomic force constants were obtained within a real-space approach, as described in more detail in Refs. [10–12]. Calculations for a $4 \times 4 \times 4$ supercell (384 atoms) were carried out with an energy cutoff of 800 eV and one $\vec{k}$-point at an equilibrium lattice parameter of 4.3033 Å. The nonanalytic contributions to the dynamical matrix in the limit of vanishing wave vector $\vec{k} \to 0$ were taken into account following the procedure given in Ref. [13]. Starting from the ideal crystal structure, different defect structures were realized within a $4 \times 4 \times 4$ supercell (383 atoms). For each cell, a relaxation of the internal coordinates was performed at an energy cutoff of 300 eV and one $\vec{k}$-point until forces were smaller than 5×10^{-2} eV/Å.

III. VIBRATIONS IN CUPROUS OXIDE

Cuprous oxide Cu_2O crystallizes in a cubic structure of space group O_h^4 ($Pn\bar{3}m$) [14–18]. Its unit cell contains two Cu_2O units, i.e., six atoms, yielding 15 optical phonon modes in addition to the three acoustic lattice vibrations. The symmetries of the vibrational modes at $k = 0$ are

$$A_{2u} \oplus E_u \oplus T_{2g} \oplus 3T_{1u} \oplus T_{2u}. \quad (1)$$

Phonons with A, E, and T symmetry are one-, two- and threefold-degenerate, respectively. The three acoustic phonons possess T_{1u} symmetry. The two remaining modes of T_{1u} symmetry are infrared active optical lattice vibrations. Phonons with A_{2u}, E_u, and T_{2u} symmetry are silent modes, neither Raman nor infrared active. The only Raman active lattice vibrations in Cu_2O belong to the threefold-degenerate T_{2g} symmetry.

According to the group theoretical analysis, the Raman spectrum of a perfect Cu_2O crystal should exhibit one one-phonon Raman signal only, that of the threefold-degenerate T_{2g} mode. However, a typical Raman spectrum of cuprous oxide is much richer with a multitude of Raman signals that have been assigned to different one-phonon scattering processes in addition to a background due to two-phonon scattering. As depicted in Fig. 1(a), such spectra are almost independent of the method and conditions of the synthesis of crystalline Cu_2O material. The spectra shown are taken of different Cu_2O samples, i.e., a natural bulk crystal, an oxidized copper sheet, as well as thin film samples grown by molecular beam epitaxy (MBE), chemical vapor epitaxy (CVD), ion-beam sputtering, and radiofrequency sputtering (rf sputtering). Very similar spectra of bulk Cu_2O crystals are reported in the literature [19–26]. It is worth noting that the Raman spectra in the literature vary slightly in the mode intensities and the number of modes observed. The reasons are manifold, for example, different scattering geometries and polarization conditions [20], different excitation conditions (i.e., in resonance and off resonance with the excitonic transitions of Cu_2O) [23], surface treatment [24], or ion-implantation [25] of the samples. However, the main findings are always the same: One observes all lattice modes in the Raman spectra of Cu_2O summarized in Table I. The Raman lattice modes observed in the spectra are in contradiction to the nominal Raman activities also given in the table.

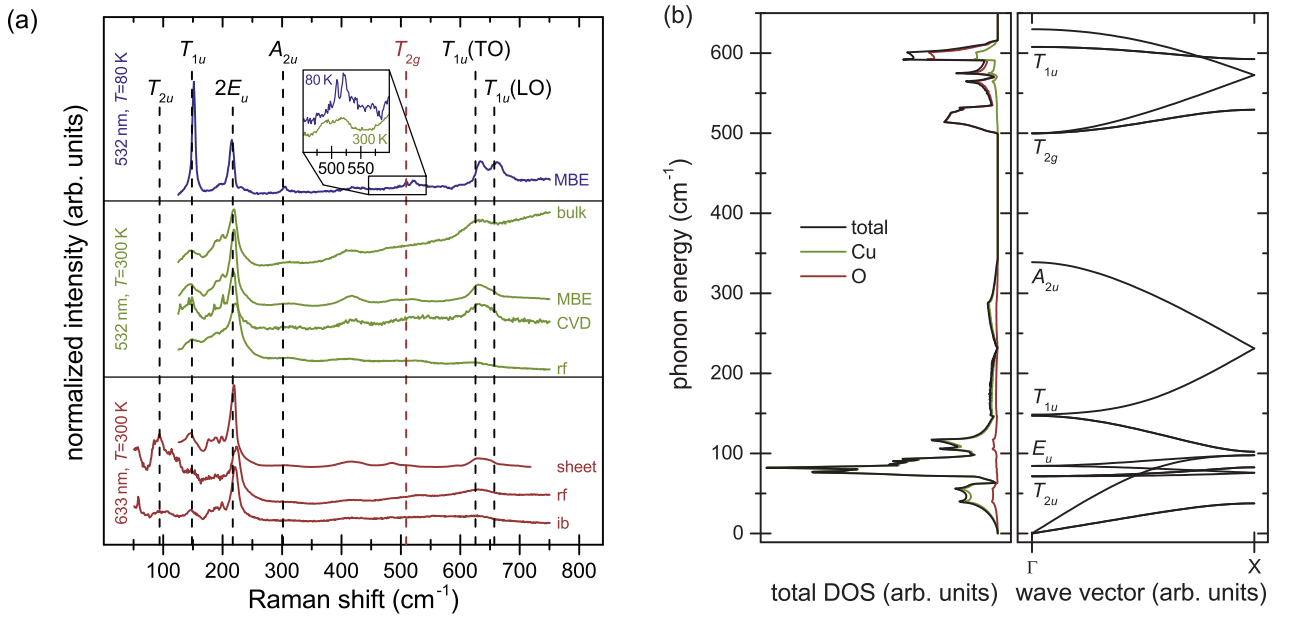

FIG. 1. (Color online) (a) Raman spectra of Cu_2O samples grown by various methods. The Raman signals are labeled according to the irreducible representations of the corresponding phonon modes in O_h symmetry. The inset shows the splitting of the T_{2g} mode at low temperatures of the MBE grown sample. For clarity, the Raman spectra are shifted on the y axis. (b) Calculated total phonon DOS and dispersion relation of Cu_2O.

TABLE I. Symmetry types and characteristic Raman shifts of lattice vibrations observed in Raman spectra of cuprous oxide in comparison to Raman shifts obtained by DFT calculations [19–26].

Mulliken symbol	Degeneracy	Experiment Raman shift (cm^{-1})	DFT Raman shift (cm^{-1})	Nominal activity
T_{2u}	3	85–100	71	silent
E_u	2	107–110	84	silent
T_{1u} (TO)	2	140–152	147	infrared
T_{1u} (LO)	1	150–160	148	infrared
A_{2u}	1	308–350	338	silent
T_{2g}	3	515	499	Raman
T_{1u} (TO)	2	608–635	608	infrared
T_{1u} (LO)	1	650–665	630	infrared

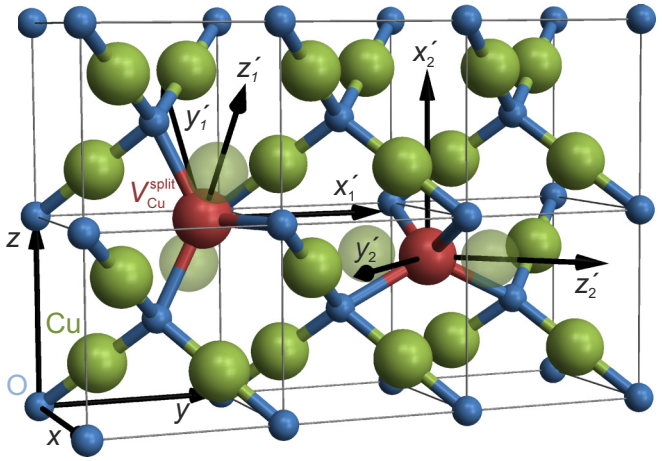

FIG. 2. (Color online) Schematic illustration of six primitive unit cells of Cu_2O with two V_{Cu}^{split} point defects occupying different lattice sites belonging to the same Wyckoff position f. The orientation of the coordinate axes $(x_1'y_1'z_1')$ and $(x_2'y_2'z_2')$ corresponding to the orthorhombic site symmetry is given with respect to the axes (xyz) of the cubic crystal structure. Green transparent atoms denote the original lattice sites of the copper atoms in the unperturbed ideal crystal structure.

IV. BREAKING OF SELECTION RULES

A number of theoretical studies published deal with the formation energies of intrinsic defects in Cu_2O as well as their electronic properties [27–33]. Intrinsic point defects that may occur comprise oxygen vacancies V_O, copper vacancies V_{Cu}, two types of oxygen interstitials $O_{i,oct}$ and $O_{i,tetr}$ with six and four Cu neighbors, respectively, the antisite defects Cu_O and O_{Cu}, and finally a copper vacancy in the so-called split configuration V_{Cu}^{split}, where a Cu atom adjacent to the vacancy moves into a position between the corresponding two Cu lattice sites. All studies agree that the V_{Cu} and V_{Cu}^{split} are most likely responsible for the natural p-type conductivity of Cu_2O as their formation energy is lower than that of other possible intrinsic acceptors such as the oxygen interstitials $O_{i,oct}$ and $O_{i,tetr}$. Thus, V_{Cu} and/or V_{Cu}^{split} are always present in this intrinsically p-type oxide.

The defects are located at specific sites of the unit cell of the Cu_2O crystal possessing a characteristic site symmetry. A set of equivalent points within the unit cell possessing the same site symmetry is associated with a Wyckoff position. The multiplicity of a Wyckoff position denotes the number of equivalent points within the unit cell. The site symmetry group is isomorphic to a subgroup of the point group to which the space group of the crystal belongs. The unit cell of Cu_2O contains two oxygen atoms (Wyckoff position a) and four copper atoms (Wyckoff position b). Thus, the antisite and vacancy point defects related to the oxygen and the copper positions have multiplicities of 2 and 4, respectively. Oxygen interstitial defects $O_{i,oct}$ and $O_{i,tetr}$ are located at Wyckoff positions c and d having multiplicities 4 and 6, respectively. As depicted in Fig. 2, the copper split vacancy V_{Cu}^{split} is located at Wyckoff position f having a multiplicity of 12.

The symmetry of the site occupied by the point defect defines a local symmetry that is usually lower than that of the space group of the crystal. As a consequence, the selection rules for the perfect crystal, e.g., Raman selection rules for extended phonon states, do not hold strictly any longer as the presence of the defect may alter the polarizability change caused by the displacement pattern of the phonon eigenstate. The symmetry of the displacement pattern of the phonon eigenstate of the perfect crystal determines whether a mode is silent, Raman allowed, or infrared allowed. It is represented by an irreducible representation of the space group of the crystal. Reducing the symmetry to the site symmetry of a point defect may make this representation reducible, i.e., it may be expanded in terms of the irreducible representations of the point group characterizing the defect site. The irreducible representations of the point group of the defect site that occur in the expansion of the representation of the original phonon state may exhibit different behavior in terms of Raman activity (i.e., silent, Raman or infrared active) than the original mode. In particular, the expansion of an originally Raman forbidden mode may contain Raman allowed irreducible representations of the point group of the defect site. Thus, vibrational modes that are Raman forbidden in a perfect crystal may become Raman allowed due to the reduction of symmetry caused by the point defect. In the case of degenerate modes, the expansion may be a sum of different irreducible representations, e.g., formerly triply degenerate T modes may be represented by a sum of an A mode and a doubly degenerate E mode. This can be taken as an indication that the degeneracy of the mode is lifted and that it may split into modes of different frequencies. It should be noted that group theory based on symmetry arguments only states whether phonon modes couple to electromagnetic radiation, but it cannot predict the magnitude of these effects. The magnitudes depend entirely on the strength of the perturbation caused by the defect.

A first group theoretical analysis of this kind has been performed by Reydellet *et al.* for substitutional defects on copper and oxygen sites of Cu_2O [19]. For V_O or Cu_O defects, all experimentally observed lattice vibrations, except the former T_{2u} mode of the perfect crystal, are activated in Raman scattering from the Γ point. The T_{2u} mode can only be activated in Raman scattering from M, R, or X points. The rather flat dispersion relation of the T_{2u} phonon branch and its nonzero phonon density of states (DOS) at the X point shown in Fig. 1(b) at first sight support the interpretation of

defect-activated scattering by zone edge phonons. However, the question remains why the corresponding breakdown of the wave vector selection rules should occur for this particular mode only or, even more severely, why it should be present in a crystalline material of good quality at all and this to an extent typical for an amorphous material. By extending and refining the analysis of Reydellet *et al.*, we will show in the following that the additional assumption of a rigorous lifting of the wave vector selection rules is not necessary to describe the Raman spectra observed.

Therefore, we extend the group theoretical analysis to other recently predicted intrinsic point defects of Cu_2O, which are likely to form according to theory. In particular, these are two types of oxygen interstitials and the copper vacancy in split configuration. Table II summarizes the results of the analysis of the effect of intrinsic point defects of Cu_2O on the defect-induced Raman activity of the extended phonon modes at the Γ point ($k \approx 0$) of the ideal crystal. Bold printed representations indicate Raman allowed modes. The irreducible representations given in the header of the table are those valid in O_h symmetry of the perfect crystal. The columns below the original representation in O_h symmetry show its expansions in terms of the irreducible representations of the point groups representing the site symmetry of the various intrinsic defects. The irreducible representations stand for the behavior of the corresponding phonon modes.

Point defects on copper sites (Wyckoff position b), i.e., V_{Cu} and O_{Cu}, as well as the oxygen interstitial $O_{i,oct}$ (Wyckoff position c) possess D_{3d} site symmetry and have the smallest impact on the Raman spectra. The vibrational modes, which are Raman forbidden in the ideal crystal, remain Raman forbidden, whereas the representation T_{2g} of the Raman active mode is expanded into the two Raman allowed irreducible representations A_{1g} and E_g of D_{3d}. The point defects V_O and Cu_O related to the oxygen sites of the unit cell (Wyckoff position a) lift the Raman forbiddance for all phonon modes at Γ with the exception of the former T_{2u} mode, which, however, shows a prominent feature at about 90 cm^{-1} in Raman spectra of Cu_2O. Point defects on oxygen sites do not introduce mode splitting because of the still rather high T_d site symmetry. The presence of the oxygen interstitial defect $O_{i,tetr}$ in the tetragonal configuration (Wyckoff position d) introduces Raman activity for all Cu_2O extended phonon modes at the Γ point. In addition, all originally degenerate modes split, i.e., the original E_u mode into A_1 and B_1, and each original T mode into a sum of a twofold-degenerated E mode and a A_2 or B_2 mode. Except for the A_2 mode all phonons are Raman active in D_{2d} symmetry. Similarly the presence of the V_{Cu}^{split} point defect introduces Raman activity for all Cu_2O extended phonon modes at the Γ point. All originally degenerate modes split, i.e., the original E_u mode into two A modes and each original T mode into a sum of B_1, B_2, and B_3 modes. Thus, V_{Cu}^{split} and $O_{i,tetr}$ are both possible candidates to introduce Raman activity of all one-phonon modes of Cu_2O. By the analysis of the angle dependence of the Raman signals in the following Sec. V, we are able to distinguish between them and to prove that the V_{Cu}^{split} defect is responsible for the effects observed.

V. ANGLE- AND POLARIZATION-DEPENDENT RAMAN SPECTROSCOPY

It is well established that polarization- and angle-dependent measurements of the intensity of one-phonon Raman signals in crystalline samples allow one to unambiguously determine the symmetry character of the corresponding Raman active lattice modes according to the space group of the crystal [34]. In this case, the scattered intensity in a Raman experiment is given by

$$I_s(M) \propto \left| \vec{e}_i^{\,T} \cdot \boldsymbol{\mathcal{R}}^M \cdot \vec{e}_s \right|^2, \tag{2}$$

where $\vec{e}_i$ and $\vec{e}_s$ are the unit vectors representing the polarization of the incident and scattered radiation, respectively, and $\boldsymbol{\mathcal{R}}(M)$ is the complex second-rank Raman tensor of mode M given in the coordinate system belonging to the crystal class of the material under study [2]. If modes are degenerate, the

TABLE II. Properties of the various intrinsic defects in Cu_2O and expansion of the irreducible representations of the O_h group in terms of the irreducible representations of the point groups representing the site symmetry of the defects. For Raman allowed modes, printed in bold, the theoretical angle dependence is given for a rotation around the x axis of a cubic crystal. Cells marked by "nd" have not been determined.

Point defect						Representations of the vibrational modes at the Γ point of Cu_2O in terms of irreducible representations of the site symmetry				
Symbol	Wyckoff position	Multiplicity	Site symmetry	Crystal class	Scattering orientation	A_{2u}	E_u	$\boldsymbol{T}_{2g}$	T_{1u}	T_{2u}
V_O, Cu_O	a	2	T_d	cubic		$\boldsymbol{A}_1$	$\boldsymbol{E}$	$\boldsymbol{T}_2$	$\boldsymbol{T}_2$	T_1
					$\vec{e}_i \parallel \vec{e}_s$	constant	constant	$\lvert\sin(2\phi)\rvert^2$	$\lvert\sin(2\phi)\rvert^2$	
					$\vec{e}_i \perp \vec{e}_s$	0	0	$\lvert\cos(2\phi)\rvert^2$	$\lvert\cos(2\phi)\rvert^2$	
V_{Cu}, O_{Cu}	b	4	D_{3d}	trigonal		A_{2u}	E_u	$\boldsymbol{A}_{1g} \oplus \boldsymbol{E}_g$	$A_{2u} \oplus E_u$	$A_{1u} \oplus E_u$
$O_{i,oct}$	c	4	D_{3d}	trigonal		A_{2u}	E_u	$\boldsymbol{A}_{1g} \oplus \boldsymbol{E}_g$	$A_{2u} \oplus E_u$	$A_{1u} \oplus E_u$
					$\vec{e}_i \parallel \vec{e}_s$			nd		
					$\vec{e}_i \perp \vec{e}_s$			nd		
$O_{i,tetr}$	d	6	D_{2d}	tetragonal		$\boldsymbol{A}_1$	$\boldsymbol{A}_1 \oplus \boldsymbol{B}_1$	$\boldsymbol{B}_2 \oplus \boldsymbol{E}$	$\boldsymbol{B}_2 \oplus \boldsymbol{E}$	$A_2 \oplus \boldsymbol{E}$
					$\vec{e}_i \parallel \vec{e}_s$	$\lvert\cos(2\phi)\rvert^2$	$\lvert\cos(2\phi)\rvert^2$	$\lvert\sin(2\phi)\rvert^2$	$\lvert\sin(2\phi)\rvert^2$	$\lvert\sin(2\phi)\rvert^2$
					$\vec{e}_i \perp \vec{e}_s$	$\lvert\sin(2\phi)\rvert^2$	$\lvert\sin(2\phi)\rvert^2$	$\lvert\cos(2\phi)\rvert^2$	$\lvert\cos(2\phi)\rvert^2$	$\lvert\cos(2\phi)\rvert^2$
V_{Cu}^{split}	f	12	D_2	orthorhombic		$\boldsymbol{A}$	$2\boldsymbol{A}$	$\boldsymbol{B}_1 \oplus \boldsymbol{B}_2 \oplus \boldsymbol{B}_3$	$\boldsymbol{B}_1 \oplus \boldsymbol{B}_2 \oplus \boldsymbol{B}_3$	$\boldsymbol{B}_1 \oplus \boldsymbol{B}_2 \oplus \boldsymbol{B}_3$
					$\vec{e}_i \parallel \vec{e}_s$	$\lvert\cos(2\phi)\rvert^2$	$\lvert\cos(2\phi)\rvert^2$	$\lvert\sin(2\phi)\rvert^2$	$\lvert\cos(2\phi)\rvert^2$	$\lvert\cos(2\phi)\rvert^2$
					$\vec{e}_i \perp \vec{e}_s$	$\lvert\sin(2\phi)\rvert^2$	$\lvert\sin(2\phi)\rvert^2$	$\lvert\cos(2\phi)\rvert^2$	$\lvert\sin(2\phi)\rvert^2$	$\lvert\sin(2\phi)\rvert^2$

total scattered intensity is found by summing the intensities corresponding to the various Raman tensors of the same mode. The rotational dependence of the phonon intensity can be calculated by parametrizing the polarization vectors in polar coordinates, i.e., one obtains for the T_{2g} mode in an ideal Cu_2O crystal for a rotation around the x axis $[x(yy)\bar{x} \leftrightarrow x(zz)\bar{x}]$

$$I_s^{||}(T_{2g}) \propto \left| \begin{pmatrix} 0 \\ \cos(\phi) \\ \sin(\phi) \end{pmatrix}^T \begin{pmatrix} 0 & 0 & 0 \\ 0 & 0 & d \\ 0 & d & 0 \end{pmatrix} \begin{pmatrix} 0 \\ \cos(\phi) \\ \sin(\phi) \end{pmatrix} \right|^2$$

$$\propto |\sin(2\phi)|^2,$$

where ϕ is the angle between the z axis and the polarization vector. A similar analysis for crossed polarizations and rotation around the x axis $[x(yz)\bar{x} \leftrightarrow x(zy)\bar{x}]$ yields $I_s^{\perp}(T_{2g}) \propto |\cos(2\phi)|^2$.

Corresponding Raman experiments have been carried out for the prominent one-phonon modes of the MBE grown Cu_2O sample with (100) orientation. The Raman spectra have been recorded in backscattering geometry at room temperature using a 532 nm laser for excitation. The Raman mode intensities versus the rotation angle are shown in Fig. 3. The angle dependence of the T_{2g} mode observed for parallel and crossed polarizations of incoming and scattered light follow the $|\sin(2\phi)|^2$ and $|\cos(2\phi)|^2$ dependence, respectively, predicted for the perfect crystal. It is also found in the experiment that the intensities of the T_{1u} and A_{2u} modes, which are Raman forbidden in perfect symmetry, as well as that of the two-phonon signal $2E_u$ exhibit an angle dependence, i.e., $|\cos(2\phi)|^2$ and $|\sin(2\phi)|^2$ dependence for parallel and crossed polarizations of incoming and scattered light, respectively.

Obviously, the angle dependence of the intensities of the modes that are forbidden in an ideal crystal cannot be explained based on the considerations made above for perfect crystal symmetry. The analysis needs to be extended to account for perturbations by point defects that introduce Raman activity of modes (which are otherwise Raman forbidden in the ideal crystal) by reducing the local symmetry. The idea is based on the picture that a point defect on a lattice site affects only its vicinity that corresponds to a well-defined volume fraction of the crystal. If the volume fractions perturbed by the defects add up to a considerable part of the entire crystal volume, the defect-induced Raman activity of extended lattice modes should become visible in the spectra. Raman tensors can be defined for each of these volume fractions and be used to calculate the contribution to the Raman spectrum of the entire crystal.

Let us assume that the crystal can be divided up into such volume fractions where each is affected by a point defect belonging to the same Wyckoff position. To calculate the corresponding rotational dependence of the intensities of the defect-activated Raman modes, one has to consider the representation of the Raman tensors in the point group of the site symmetry. The orientation of the axis of rotation $\vec{r}$ is then defined with respect to the basis axes of the coordinate system given by the local site symmetry. The conventions for the choice of the basis axes in relation to the characteristic symmetry elements of each crystal class are given in the book by Nye [35]. Examples are shown in Fig. 2 for two V_{Cu}^{split} sites embedded in cubic Cu_2O. The coordinate system describing the cubic structure is given by (xyz). The two coordinate systems $(x_1'y_1'z_1')$ and $(x_2'y_2'z_2')$ correspond to the two V_{Cu}^{split} defects depicted. Although the two sites belong to the same Wyckoff position f and thus possess the same orthorhombic site symmetry, the local coordinate frames $(x_1'y_1'z_1')$ and $(x_2'y_2'z_2')$ representing the orthorhombic system are different. In each case, one obtains for the scattered intensities

$$I_s(M) \propto \left| [\boldsymbol{R}(\vec{r},\phi)\boldsymbol{T}\vec{e}_i]^T \cdot \boldsymbol{\mathcal{R}}^M \cdot [\boldsymbol{R}(\vec{r},\phi)\boldsymbol{T}\vec{e}_s] \right|^2, \quad (3)$$

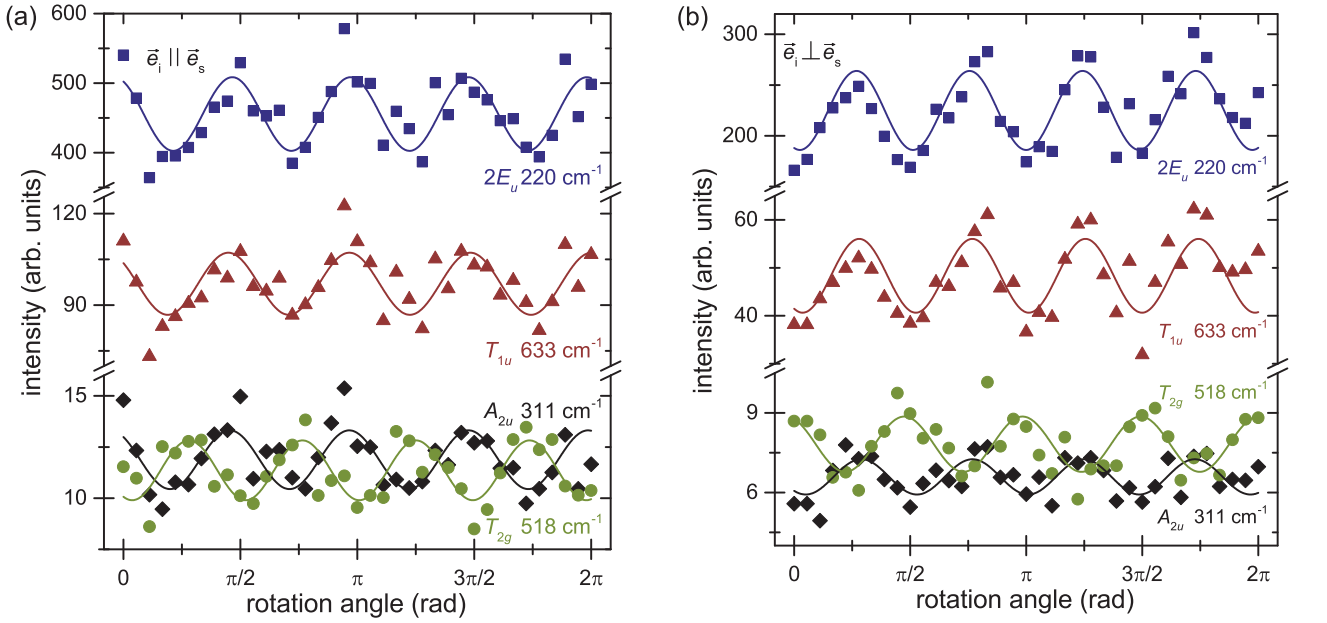

FIG. 3. (Color online) (a) Raman mode intensities vs rotation angle for a rotation around the x axis $[x(yy)\bar{x} \leftrightarrow x(zz)\bar{x}]$ of a MBE grown Cu_2O sample with (100) orientation for parallel orientated polarization vectors of the incident and scattered radiation. (b) Intensity dependencies for crossed polarization vectors $[x(yz)\bar{x} \leftrightarrow x(zy)\bar{x}]$. Solid lines are guides to the eye.

where $\boldsymbol{T}$ describes the coordinate transformation between the global coordinates (xyz) of ideal cubic Cu_2O and the local coordinates belonging to the symmetry of the defect site. $\boldsymbol{R}$ denotes the rotation around a vector $\vec{r}$ (here the normal vector of the (100) plane of Cu_2O) by an angle ϕ. If the definition of the basis axes differs for the multiple sites belonging to the same Wyckoff position, averaging of the intensities over the different orientations is required. For simplicity, we have assumed that the defects are evenly distributed on the equivalent sites of the corresponding Wyckoff position.

The results of such calculations are given in Table II for each defect for parallel as well as perpendicular aligned polarization vectors, except for the D_{3d} symmetry, for which it was not possible to define a local coordinate system. The intensity dependence of the modes observed in our experiment cannot be described correctly by defect-induced Raman activity caused by substitutional or interstitial defects. In particular, the $O_{i,tetr}$ interstitial for which all one-phonon modes become Raman allowed does not yield the correct angle dependence. Only the copper split vacancy yields the correct angle dependence for all one-phonon modes analyzed if appropriate tensor elements are chosen. The original T_{1u} and T_{2u} modes can be represented by a sum of the averaged intensities of all three B modes, whereas at the same time the T_{2g} phonon is given correctly with respect to the experimental findings by a sum of B_1 and B_3 modes implying that the B_2 tensor elements are zero. In this fashion, the angle dependence of the Raman signal corresponding to the T_{2g} mode of the perfect crystal can be preserved in the presence of the V_{Cu}^{split} point defect.

The angle dependence of the $2E_u$ two-phonon signal can be estimated considering the expansion of the direct product $E_u \otimes E_u = \boldsymbol{A}_{1g} \oplus A_{2g} \oplus \boldsymbol{E}_g$ for the ideal crystal (O_h symmetry). The expansion corresponds to $4\boldsymbol{A}$ in D_2 symmetry, i.e., in the site symmetry of the copper split vacancy. Hence, the $2E_u$ signal should exhibit the same angle dependence as the A_{2u} one-phonon signal in the experiment. This is the case as shown in Fig. 3. The behavior of the $2E_u$ signal is thus in agreement with the interpretation that the Raman activity of Cu_2O phonon modes is determined by the V_{Cu}^{split} defects.

The defect-induced mode splittings, which may occur on reducing the symmetry, appear to be rather small. Thus, at room temperature, the Raman signals assigned to the one-phonon Raman signals of ideal Cu_2O can be fitted by single oscillators to extract the intensities as a function of rotation angle and to compare them with the corresponding group theoretical results, as was done in the analysis presented in Fig. 3. However, at low temperatures, it can be seen that the broad signals are rather a superposition of peaks at different frequencies. In particular, the rather broad T_{2g} mode splits into two separate signals at low temperatures, as depicted in the inset of Fig. 1(a), which may be attributed to the B_1 and B_3 contributions discussed above. This is a further confirmation of our interpretation.

VI. MAGNITUDE OF THE PERTURBATION

Our Raman analysis above implies that the copper split vacancy causes a much stronger perturbation of the Cu_2O crystal than any other point defect in Cu_2O. To estimate the magnitude of the crystal perturbation, DFT calculations

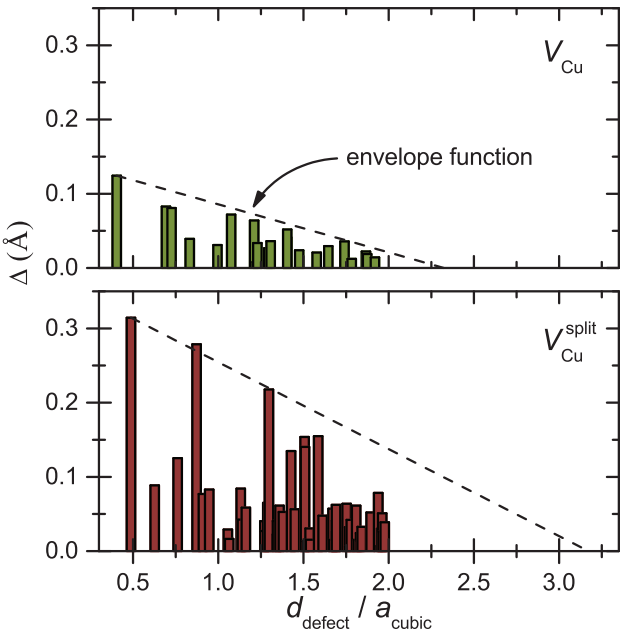

FIG. 4. (Color online) Shift Δ of atoms surrounding the V_{Cu} (upper diagram) and the V_{Cu}^{split} defect (lower diagram) upon relaxation vs distance from the respective defect in units of the cubic lattice constant a_{cubic}. The split vacancy influences atoms at distances much larger than a_{cubic}, whereas V_{Cu} only induces comparably small perturbations. Dashed lines are envelope functions of the Δ values.

for supercell defect structures were conducted as outlined in Sec. II. We used the GGA-PBE functional to describe the relaxation of the internal coordinates. As discussed in Ref. [32], one has to resort to hybrid-functional techniques in order to achieve an accurate description of the electronic structure and defect formation energies. However, in a recent letter we have shown that standard functionals such as the LDA+U lead to reasonable descriptions of structural properties of copper oxide phases [36]. Moreover, the cubic lattice constant of 4.3033 Å and the Cu-O bond length of 1.86 Å obtained from the GGA-PBE functional applied here are in good agreement with experiment [37]. We expect the GGA to give reasonable results since we are only interested in the forces induced by introducing defects in the ideal cuprite structure and resulting atomic shifts upon relaxation.

Figure 4 gives an estimate of the spatial extension and of the magnitude of the perturbations caused by V_{Cu} and V_{Cu}^{split}, respectively, by looking at the shift Δ of the positions of the atoms surrounding the defects upon relaxation with respect to the unperturbed structure. The shift Δ is obtained as the norm of the difference vector of each atom position between the relaxed perturbed and unperturbed structure. It is evident that the shifts of the positions of the atoms surrounding a V_{Cu}^{split} are considerably larger than the corresponding shifts of the same atoms surrounding a V_{Cu} instead. For example, at a distance of about $1.5a_{cubic}$, the shift introduced by the V_{Cu}^{split} is more than six times larger than that of the V_{Cu} defect. This suggests that the perturbation caused by V_{Cu}^{split}, which comprises several sites, is much stronger than that caused by simple point defects involving only one atom site such as V_{Cu} shown here, or substitutional or interstitial defects.

Furthermore, assuming that the envelope of the Δ values is a straight line (dashed line in Fig. 4) and that its point of interception with the $d_{\text{defect}}/a_{\text{cubic}}$ axis is a rough measure of the spatial extension of the defect, i.e., it corresponds to the radius of the volume fraction affected by the defect site, one obtains for $V_{\text{Cu}}^{\text{split}}$ and V_{Cu} values of $3.2a_{\text{cubic}}$ and $2.3a_{\text{cubic}}$, respectively, indicating that the perturbation caused by $V_{\text{Cu}}^{\text{split}}$ is not only stronger than that of V_{Cu}, but also of a longer range. Finally, the density of atoms in Cu_2O is about 7.5×10^{22} atoms/cm^3. If we assume that the volume fraction of the crystal perturbed by a $V_{\text{Cu}}^{\text{split}}$ is a spherical volume with a radius of $3.2a_{\text{cubic}}$, it will contain about 825 atoms. Thus, the volume fractions perturbed by $V_{\text{Cu}}^{\text{split}}$ defects in their centers make up the entire crystal volume at a critical defect density of about 9.1×10^{19} defects/cm^3. This number is about $10\times$ the typical density of $V_{\text{Cu}}^{\text{split}}$ expected, implying that 10% of the crystal is strongly perturbed. This appears to be sufficient to yield additional signals and is in agreement with our explanation of the origin of the unusual Raman spectrum of Cu_2O.

VII. CONCLUSIONS

In conclusion, the Raman spectrum of cuprous oxide Cu_2O is very peculiar in the sense that it is dominated by features assigned to Raman forbidden one-phonon modes of the perfect crystal. We developed a general group theoretical approach that allowed us to describe the intensity dependence of such unexpected Raman signals on sample rotation. Employing this approach to Cu_2O yields unambiguously that the Raman activity of these otherwise infrared and silent modes is induced by the presence of the copper split vacancy $V_{\text{Cu}}^{\text{split}}$. As the Raman spectrum of Cu_2O depends weakly on synthesis method and conditions, this suggests that $V_{\text{Cu}}^{\text{split}}$ point defects are always present in Cu_2O and are responsible for its intrinsic p-type conductivity, which is in agreement with recent theoretical work.

Considering material systems other than cuprous oxide, point defects may not introduce Raman activity of infrared active or silent modes since the perturbation of the site symmetry is not large enough or the crystal volume affected is too small. For instance, cubic GaAs belongs to space group T_d^2 ($F\bar{4}3m$) [38]. Its unit cell contains two atoms yielding one triply degenerate Raman active mode. Doping GaAs by Si may lead to the formation of substitutional Si_{Ga} and Si_{As} defects possessing the site symmetry T_d like the unperturbed crystal and therefore the selection rules are not altered [39]. However, localized vibrational Si modes have been reported [4]. Structures with larger unit cells often possess lattice sites with a site symmetry lower than the crystal symmetry. For example, vacancies in wurtzite materials (such as CdS or ZnO) belonging to space group C_{6v}^4 ($P6_3mc$) possess C_{3v} site symmetry and, following the analysis introduced in Sec. IV, introduce Raman activity of forbidden modes [39,40]. However, there are no generalized rules established yet when such perturbations are large enough to cause an alternation of the Raman spectra of the crystals.

ACKNOWLEDGMENTS

We are grateful to Bruno K. Meyer for fruitful discussions and for providing the CVD grown and sputtered samples. We thank Martin Eickhoff for the provision of the MBE samples.

[1] F. A. Kröger, *The Chemistry of Imperfect Crystals* (North-Holland, Amsterdam, 1964).
[2] R. Loudon, Adv. Phys. **13**, 423 (1964).
[3] A. S. Barker and A. J. Sievers, Rev. Mod. Phys. **47**, S1 (1975).
[4] M. D. McCluskey, J. Appl. Phys. **87**, 3593 (2000).
[5] R. Shuker and R. W. Gammon, Phys. Rev. Lett. **25**, 222 (1970).
[6] G. Kresse and J. Hafner, Phys. Rev. B **47**, 558 (1993).
[7] G. Kresse and J. Hafner, Phys. Rev. B **49**, 14251 (1994).
[8] G. Kresse and J. Furthmüller, Phys. Rev. B **54**, 11169 (1996).
[9] G. Kresse and J. Furthmüller, Comput. Mater. Sci. **6**, 15 (1996).
[10] M. H. F. Sluiter, M. Weinert, and Y. Kawazoe, Europhys. Lett. **43**, 183 (1998).
[11] M. H. F. Sluiter, M. Weinert, and Y. Kawazoe, Phys. Rev. B **59**, 4100 (1999).
[12] K. Esfarjani and H. T. Stokes, Phys. Rev. B **77**, 144112 (2008).
[13] X. Gonze and C. Lee, Phys. Rev. B **55**, 10355 (1997).
[14] R. J. Elliott, Phys. Rev. **124**, 340 (1961).
[15] K. Huang, Z. Phys. **171**, 213 (1963).
[16] M. Balkanski, M. Nusimovici, and J. Reydellet, Solid State Commun. **7**, 815 (1969).
[17] C. Carabatos, Phys. Status Solidi B **37**, 773 (1970).
[18] C. Carabatos and B. Prevot, Phys. Status Solidi B **44**, 701 (1971).
[19] J. Reydellet, M. Balkanski, and D. Trivich, Phys. Status Solidi B **52**, 175 (1972).
[20] A. Compaan and H. Z. Cummins, Phys. Rev. B **6**, 4753 (1972).
[21] Y. Petroff, P. Y. Yu, and Y. R. Shen, Phys. Rev. Lett. **29**, 1558 (1972).
[22] P. Dawson, M. Hargreave, and G. Wilkinson, J. Phys. Chem. Solids **34**, 2201 (1973).
[23] P. F. Williams and S. P. S. Porto, Phys. Rev. B **8**, 1782 (1973).
[24] A. Compaan, Solid State Commun. **16**, 293 (1975).
[25] D. Powell, A. Compaan, J. R. Macdonald, and R. A. Forman, Phys. Rev. B **12**, 20 (1975).
[26] K. Reimann and K. Syassen, Phys. Rev. B **39**, 11113 (1989).
[27] A. F. Wright and J. S. Nelson, J. Appl. Phys. **92**, 5849 (2002).
[28] M. A. Mäki-Jaskari, Mod. Simul. Mater. Sci. **14**, 207 (2006).
[29] M. Nolan and S. D. Elliott, Phys. Chem. Chem. Phys. **8**, 5350 (2006).
[30] H. Raebiger, S. Lany, and A. Zunger, Phys. Rev. B **76**, 045209 (2007).
[31] A. Soon, X.-Y. Cui, B. Delley, S.-H. Wei, and C. Stampfl, Phys. Rev. B **79**, 035205 (2009).
[32] D. O. Scanlon, B. J. Morgan, G. W. Watson, and A. Walsh, Phys. Rev. Lett. **103**, 096405 (2009).
[33] D. O. Scanlon, B. J. Morgan, and G. W. Watson, J. Chem. Phys. **131**, 124703 (2009).
[34] T. Sander, S. Eisermann, B. K. Meyer, and P. J. Klar, Phys. Rev. B **85**, 165208 (2012).
[35] J. F. Nye, *Physical Properties of Crystals*, 3rd ed. (Oxford University Press, London, 1957).

[36] M. Heinemann, B. Eifert, and C. Heiliger, Phys. Rev. B **87**, 115111 (2013).

[37] B. K. Meyer, A. Polity, D. Reppin, M. Becker, P. Hering, P. J. Klar, T. Sander, C. Reindl, J. Benz, M. Eickhoff, C. Heiliger, M. Heinemann, J. Bläsing, A. Krost, S. Shokovets, C. Müller, and C. Ronning, Phys. Status Solidi B **249**, 1487 (2012).

[38] S. Mitra, Phys. Lett. **11**, 119 (1964).

[39] *International Tables for Crystallography Vol. A: Space-Group Symmetry*, 5th ed., edited by T. Hahn (Springer, Dordrecht, 2005).

[40] C. A. Arguello, D. L. Rousseau, and S. P. S. Porto, Phys. Rev. **181**, 1351 (1969).